Journal of Engineering Mathematics **28**: 311–325, 1994.

Point force excitation of a thick-walled elastic infinite pipe with an embedded inhomogeneity

S. OLSSON

Division of Mechanics, Chalmers University of Technology, S-41296 Göteborg, Sweden

Received 10 May 1993; accepted in revised form 20 October 1993

Abstract. The propagation of elastic waves in a thick-walled pipe with an embedded inhomogeneity is considered. The pipe is excited by a point force applied on its surface and the time harmonic problem is solved using the null field approach, a method whose main characteristics are surface integral representations and expansions in spherical and cylindrical vector wave functions. Entering in the expression for the scattered field are the transition matrix for the cavity, the reflection matrices for the inner and outer surfaces of the pipe, the transformation functions between the spherical and cylindrical vector wave functions and also the translation functions for the cylindrical waves. Numerical examples, both in the frequency and time domain, are presented for a spherical cavity and an open circular crack.

I. Introduction

In the present paper we use the null field approach (or 'T matrix method') to investigate the propagation of time harmonic elastic waves in an infinite circular pipe with an embedded bounded inhomogeneity. The elastic medium of the pipe is assumed to be homogeneous, isotropic and linear and we excite the pipe by applying a point force on its outer surface. This is a problem of apparent interest in many applications, for example, in the detection of imperfections in materials in non-destructive evaluation.

The characteristic features of the null field approach are the use of surface integral representations containing the free space Green tensor and expansions in systems of global wave functions, in this case spherical and cylindrical vector wave functions. Details on the basic features of this method, as it applies to elastodynamic problems, can be found in [1–4], and for a brief introduction to integral representations and integral equations for time harmonic fields in general we refer to [5] (where further useful references are given). The mutiple scattering structure of the problem is then inherent in the system of equations obtained from the integral representations. With the solution of this system at hand, we can obtain the scattered displacement field in the pipe. The main constituents appearing in the solution are the transition matrix for the cavity, the reflection matrices for the cylindrical surfaces, the transformation functions between the sets of wave functions and the translation functions for the cylindrical waves.

A number of authors have treated problems that are closely related to the present one. Here we shall only mention a few that have also adopted the null field approach as their method of solution. Thus, the scattering of elastic waves by an inhomogeneity in an elastic half space and in a layered elastic half space is considered in [6–7], and an inhomogeneity in an elastic plate is treated in [8–9]. A geometrical configuration which is of particular relevance for the present article is the case of an inhomogeneity in a cylindrical structure.

This has been considered both in the acoustic [10–11] and the elastic case [12–13], but in these references, contrary to the present work, there is only one cylindrical surface involved.

In order to make the presentation as short and clear as possible, we have decided not to include the complete explicit forms for the vector wave functions and the transformation and translation functions used. Instead, we give references to where they can be found. The formal solution of the scattering problem is presented in Section II. In Section III the source, and thereby the incident field, is specified and in Section IV the numerical aspects are discussed. We consider both a spherical cavity and an open circular crack. Plots of the displacement field, both in the frequency and time domain, are presented.

II. Formal theory

Consider an infinite elastic pipe with an embedded obstacle as depicted in Fig. 1. The inner surface S_0, and outer surface S_2 of the pipe, are assumed to be circular cylinders with radii a_0 and a_2, respectively. In this section we let the obstacle, S_1, be a cavity with practically arbitrary shape (the unit normals $\hat{n}_\nu$, $\nu = 0, 1, 2$, is pointing outwards as shown). Later in the numerical applications, we will emphasise a spherical obstacle and a circular ('penny-shaped') crack. The restrictions imposed on the geometry here are not necessary for the validity of the formal theory developed in this section. For the null field approach to be applicable there must, however, exist inscribed and circumscribed circular cylinders and spheres for the appropriate surfaces which must also satisfy the requirements of the divergence theorem (these restrictions can be partially relaxed, see Section IV). Our coordinate systems are then chosen according to Fig. 1 and the vector, **d**, that separates the

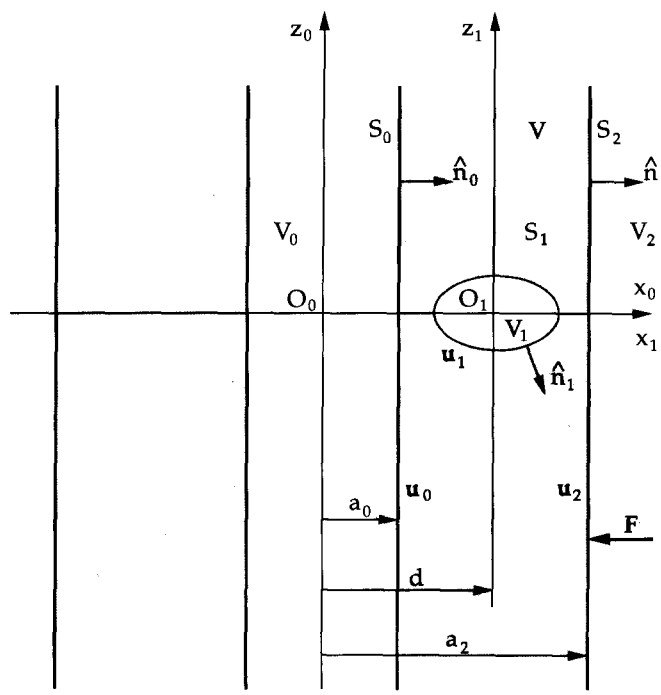

Fig. 1. Geometry and notations for a pipe with an embedded inhomogeneity and an applied point force.

origins is pointing towards O_1. Furthermore V_0 denotes the volume inside S_0, V_1 inside S_1, V_2 outside S_2 and V the volume outside S_0, inside S_2 and outside S_1. We are concentrating on time harmonic conditions and thus the time factor $\exp(-i\omega t)$ is suppressed in all formulas. The transverse and longitudinal wave numbers are $k_s^2 = \rho_0\omega^2/\mu$ and $k_p^2 = \rho_0\omega^2/(\lambda + 2\mu)$, respectively, where ρ_0 is the density and λ and μ are the Lamé constants of the elastic medium.

We study the displacement field $\mathbf{u} = \mathbf{u}^i + \mathbf{u}^s$ (incident plus scattered field) in the elastic pipe. The incident field, $\mathbf{u}^i$, is the field from the source as if no scattering surfaces were present, i.e. as if the source was located in a homogeneous space with the material properties of the pipe. The boundary conditions which we apply to the present problem are those of vanishing surface tractions, i.e.

$$\mathbf{t}(\mathbf{u}(\mathbf{r})) = \mathbf{0}\,, \qquad \mathbf{r} \in S_\nu\,, \quad \nu = 0, 1, 2\,, \tag{1}$$

where the traction $\mathbf{t}$ is defined as

$$\mathbf{t}(\mathbf{r}) = \mathbf{t}(\mathbf{u}(\mathbf{r})) = \lambda\hat{n}\,\nabla\cdot\mathbf{u}(\mathbf{r}) + 2\mu\frac{\partial\mathbf{u}(\mathbf{r})}{\partial n} + \mu\hat{n}\times(\nabla\times\mathbf{u}(\mathbf{r}))\,, \tag{2}$$

and where $\partial/\partial n$ is the normal derivative. The starting point in the null field approach is a surface integral representation for the displacement field $\mathbf{u}$ which for the present problem is

$$\begin{aligned}
&\mathbf{u}^i(\mathbf{r}') + \frac{k_s}{\mu}\int_{S_0}\{\mathbf{u}_0(\mathbf{r})\cdot(\hat{n}\cdot\Sigma(\mathbf{r},\mathbf{r}')) - \mathbf{t}_0(\mathbf{r})\cdot\mathbf{G}(\mathbf{r},\mathbf{r}')\}\,\mathrm{d}S \\
&\quad + \frac{k_s}{\mu}\int_{S_1}\{\mathbf{u}_1(\mathbf{r})\cdot(\hat{n}\cdot\Sigma(\mathbf{r},\mathbf{r}')) - \mathbf{t}_1(\mathbf{r})\cdot\mathbf{G}(\mathbf{r},\mathbf{r}')\}\,\mathrm{d}S \\
&\quad - \frac{k_s}{\mu}\int_{S_2}\{\mathbf{u}_2(\mathbf{r})\cdot(\hat{n}\cdot\Sigma(\mathbf{r},\mathbf{r}')) - \mathbf{t}_2(\mathbf{r})\cdot\mathbf{G}(\mathbf{r},\mathbf{r}')\}\,\mathrm{d}S \\
&\quad = \begin{cases}\mathbf{u}(\mathbf{r}')\,, & \mathbf{r}' \in V \\ \mathbf{0}\,, & \mathbf{r}' \in V_0, V_1 \text{ or } V_2\,.\end{cases}
\end{aligned} \tag{3}$$

Here $\mathbf{u}_\nu$, $\nu = 0, 1, 2$, are the surface displacement fields, $\mathbf{t}_\nu$, $\nu = 0, 1, 2$, the surface tractions, $\mathbf{G}(\mathbf{r},\mathbf{r}')$ the free space Green tensor and $\hat{n}\cdot\Sigma(\mathbf{r},\mathbf{r}')$ is the Green surface traction tensor which has the same relation to the Green tensor as the stress tensor has to the displacement, i.e.

$$\hat{n}\cdot\Sigma(\mathbf{r},\mathbf{r}') = \mathbf{t}(\mathbf{G}(\mathbf{r},\mathbf{r}')) = \lambda\hat{n}\,\nabla\cdot\mathbf{G}(\mathbf{r},\mathbf{r}') + 2\mu\frac{\partial\mathbf{G}(\mathbf{r},\mathbf{r}')}{\partial n} + \mu\hat{n}\times(\nabla\times\mathbf{G}(\mathbf{r},\mathbf{r}'))\,. \tag{4}$$

Applying the boundary conditions, equation (1), the second terms in the integrals in equation (3) vanish.

When working with the integral representation, equation (3), we use expansions of the Green surface traction tensor and the displacement fields in spherical or cylindrical vector wave functions. Here we only introduce the notations for these functions and for a detailed definition we refer to Ref. [13] or [14] (note, however, that for the cylindrical wave functions we use the same normalisation as in [13]). Thus, the outgoing and regular spherical vector wave functions are denoted $\boldsymbol{\psi}_n(\mathbf{r})$ and $\mathrm{Re}\,\boldsymbol{\psi}_n(\mathbf{r})$, respectively (the former contains spherical Hankel functions of the first kind, the latter spherical Bessel functions and both contain vector spherical harmonics). The index n is a multiple index that contains a mode index, τ

(SH, SV and P waves) and the three indices, σ, m, l, of the real spherical harmonics. Similarly, the outgoing and regular cylindrical vector wave functions are denoted $\boldsymbol{\chi}_k(h;\mathbf{r})$ and $\operatorname{Re}\boldsymbol{\chi}_k(h;\mathbf{r})$, respectively (they contain Hankel or Bessel functions, trigonometric functions and an exponential). The axial wave number is h and we also define the radial wave numbers $q_p=(k_p^2-h^2)^{1/2}$ and $q_s=(k_s^2-h^2)^{1/2}$ with the square roots chosen to have non-negative imaginary parts. The multiple index k stands for (τ,σ,m) and we also introduce the functions $\boldsymbol{\chi}_k^\dagger(h;\mathbf{r})$ and $\operatorname{Re}\boldsymbol{\chi}_k^\dagger(h;\mathbf{r})$ by replacing all explicit 'i' by '$-i$'. The transformations between the spherical and cylindrical wave functions are

$$\operatorname{Re}\boldsymbol{\chi}_k(h;\mathbf{r})=\sum_{n'} C^\dagger_{n'k}(h)\operatorname{Re}\boldsymbol{\chi}_{n'}(\mathbf{r}) \tag{5}$$

$$\boldsymbol{\psi}_n(\mathbf{r})=\sum_{k'}\int_{-\infty}^{\infty} C_{nk'}(h)\boldsymbol{\chi}_{k'}(h;\mathbf{r})\frac{\mathrm{d}h}{k_s},\quad \rho>0\,, \tag{6}$$

where the transformation functions $C_{nk'}(h)$ and $C^\dagger_{nk'}(h)$ (obtained from $C_{nk'}(h)$ by replacing all explicit 'i' by '$-i$') can be found in [14]. We use spherical coordinates (r,θ,φ) and cylindrical coordinates (ρ,φ,z). Since we are working with two different cylindrical coordinate systems, we also need the translation properties for the cylindrical wave functions

$$\operatorname{Re}\boldsymbol{\chi}_k(h;\mathbf{r}_0)=\sum_{k'} R_{kk'}(h;\mathbf{d})\operatorname{Re}\boldsymbol{\chi}_{k'}(h;\mathbf{r}_1) \tag{7}$$

$$\boldsymbol{\chi}_k(h;\mathbf{r}_0)=\sum_{k'} P_{kk'}(h;\mathbf{d})\operatorname{Re}\boldsymbol{\chi}_{k'}(h;\mathbf{r}_1)\,, \tag{8}$$

where $\mathbf{r}_0=\mathbf{d}+\mathbf{r}_1$ (the index 0 or 1 on the radius vector of course relates to the origin O_0 or O_1). The translation functions $R_{kk'}(h;\mathbf{d})$ and $P_{kk'}(h;\mathbf{d})$ are also given in [14]. From the Green tensor expansions (cf. [14]) we can also derive the above-mentioned expansions of the Green surface traction tensor which in our notation become

$$\hat{n}\cdot\boldsymbol{\Sigma}(\mathbf{r},\mathbf{r}')=\begin{cases} i\sum_n \operatorname{Re}\boldsymbol{\psi}_n(\mathbf{r}')\,\mathbf{t}(\boldsymbol{\psi}_n(\mathbf{r}))\,, & r'<r\\ i\sum_n \boldsymbol{\psi}_n(\mathbf{r}')\,\mathbf{t}(\operatorname{Re}\boldsymbol{\psi}_n(\mathbf{r}))\,, & r'>r\end{cases} \tag{9}$$

$$\hat{n}\cdot\boldsymbol{\Sigma}(\mathbf{r},\mathbf{r}')=\begin{cases} i\sum_k \int_{-\infty}^{\infty}\operatorname{Re}\boldsymbol{\chi}_k(h;\mathbf{r}')\,\mathbf{t}(\boldsymbol{\chi}_k^\dagger(h;\mathbf{r}))\frac{\mathrm{d}h}{k_s}, & \rho'<\rho\\ i\sum_k \int_{-\infty}^{\infty}\boldsymbol{\chi}_k(h;\mathbf{r}')\,\mathbf{t}(\operatorname{Re}\boldsymbol{\chi}_k^\dagger(h;\mathbf{r}))\frac{\mathrm{d}h}{k_s}, & \rho'>\rho\,.\end{cases} \tag{10}$$

For the incident field we need three different expansions

$$\mathbf{u}^i(\mathbf{r}')=\sum_k\int_{-\infty}^{\infty} a_k^0(h)\operatorname{Re}\boldsymbol{\chi}_k(h;\mathbf{r}_0')\frac{\mathrm{d}h}{k_s},\quad \mathbf{r}'\in V_0 \tag{11}$$

$$\mathbf{u}^i(\mathbf{r}')=\sum_n a_n\operatorname{Re}\boldsymbol{\psi}_n(\mathbf{r}_1')\,,\qquad \mathbf{r}'\in V_1 \tag{12}$$

$$\mathbf{u}^i(\mathbf{r}')=\sum_k\int_{-\infty}^{\infty} a_k^2(h)\boldsymbol{\chi}_k(h;\mathbf{r}_0')\frac{\mathrm{d}h}{k_s},\qquad \mathbf{r}'\in V_2\,, \tag{13}$$

where the coefficients $a_k^0(h)$, $a_k^2(h)$ and a_n are considered to be known quantities. Finally, we assume the following expansions for the surface fields on S_0, S_1 and S_2

$$\mathbf{u}_0(\mathbf{r}) = \sum_k \int_{-\infty}^{\infty} \gamma_k^0(h)\, \mathrm{Re}\, \boldsymbol{\chi}_k(h;\mathbf{r}_0)\, \frac{\mathrm{d}h}{k_s}, \quad \mathbf{r} \in S_0 \tag{14}$$

$$\mathbf{u}_1(\mathbf{r}) = \sum_n \beta_n\, \mathrm{Re}\, \boldsymbol{\psi}_n(\mathbf{r}_1), \qquad \mathbf{r} \in S_1 \tag{15}$$

$$\mathbf{u}_2(\mathbf{r}) = \sum_k \int_{-\infty}^{\infty} \gamma_k^2(h)\, \mathrm{Re}\, \boldsymbol{\chi}_k(h;\mathbf{r}_0)\, \frac{\mathrm{d}h}{k_s}, \quad \mathbf{r} \in S_2. \tag{16}$$

The integral representation, equation (3), for the displacement field $\mathbf{u}$ is now employed for the four regions V, V_0, V_1 and V_2. The field expansions according to equations (11)–(16) are inserted and the appropriate expansions of the Green surface traction tensor are utilized (i.e. in the integral over S_1 we use an expansion in spherical vector waves according to equation (9) and in the integrals over S_0 and S_2 we expand in cylindrical waves according to equation (10)). Furthermore, $\boldsymbol{\psi}_n(\mathbf{r}_1')$ is transformed and translated into $\mathrm{Re}\, \boldsymbol{\chi}_k(h;\mathbf{r}_0')$ in V_0, $\boldsymbol{\psi}_n(\mathbf{r}_1')$ is transformed and translated into $\boldsymbol{\chi}_k(h;\mathbf{r}_0')$ in V_2 and both $\boldsymbol{\chi}_k(h;\mathbf{r}_0')$ and $\mathrm{Re}\, \boldsymbol{\chi}_k(h;\mathbf{r}_0')$ are translated and transformed (note the order of the operations) into $\mathrm{Re}\, \boldsymbol{\psi}_n(\mathbf{r}_1')$ in V_1. Employing the linear independence of the spherical and cylindrical waves inside a sphere and outside or inside a cylinder, we in turn get for the four regions V_0, V_2, V_1 and V

$$a_k^0(h) + i \sum_{k'} \frac{1}{k_s} \gamma_{k'}^0(h) Q_{kk'}^0(h) - i \sum_{k'} \frac{1}{k_s} \gamma_{k'}^2(h) Q_{kk'}^2(h) + i \sum_{k'n''n'''} C_{n''k'}(h) P_{k'k}(h;-\mathbf{d})\, \mathrm{Re}\, Q_{n''n'''} \beta_{n'''} = 0, \tag{17}$$

$$a_k^2(h) + i \sum_{k'} \frac{1}{k_s} \gamma_{k'}^0(h)\, \mathrm{Re}\, Q_{kk'}^0(h) - i \sum_{k'} \frac{1}{k_s} \gamma_{k'}^2(h)\, \mathrm{Re}\, Q_{kk'}^2(h) + i \sum_{k'n''n'''} C_{n''k'}(h) R_{k'k}(h;-\mathbf{d})\, \mathrm{Re}\, Q_{n''n'''} \beta_{n'''} = 0, \tag{18}$$

$$a_n + i \sum_{k'k''k'''} \int_{-\infty}^{\infty} \frac{\mathrm{d}h}{k_s} P_{k'k''}(h;\mathbf{d}) C_{nk''}^{\dagger}(h) \frac{1}{k_s} \gamma_{k'''}^0(h)\, \mathrm{Re}\, Q_{k'k'''}^0(h) + i \sum_{k'k''k'''} \int_{-\infty}^{\infty} \frac{\mathrm{d}h}{k_s} R_{k'k''}(h;\mathbf{d}) C_{nk''}^{\dagger}(h) \frac{1}{k_s} \gamma_{k'''}^2(h) Q_{k'k'''}^2(h) + i \sum_{n'} Q_{nn'} \beta_{n'} = 0, \tag{19}$$

$$\mathbf{u}^s(\mathbf{r}') = \mathbf{u}(\mathbf{r}') - \mathbf{u}^i(\mathbf{r}') = i \sum_{kk'} \int_{-\infty}^{\infty} \frac{\mathrm{d}h}{k_s} \boldsymbol{\chi}_k(h;\mathbf{r}_0') \frac{1}{k_s} \gamma_{k'}^0(h)\, \mathrm{Re}\, Q_{kk'}^0(h) - i \sum_{kk'} \int_{-\infty}^{\infty} \frac{\mathrm{d}h}{k_s}\, \mathrm{Re}\, \boldsymbol{\chi}_k(h;\mathbf{r}_0') \frac{1}{k_s} \gamma_{k'}^2(h) Q_{kk'}^2(h) + i \sum_{nn'} \boldsymbol{\psi}_n(\mathbf{r}_1')\, \mathrm{Re}\, Q_{nn'} \beta_{n'}. \tag{20}$$

Here we have introduced

$$Q_{kk'}^0(h,h') = \frac{k_s}{\mu} \int_{S_0} \mathrm{Re}\, \boldsymbol{\chi}_{k'}(h';\mathbf{r}_0) \cdot \mathbf{t}(\boldsymbol{\chi}_k^{\dagger}(h;\mathbf{r}_0))\, \mathrm{d}S, \tag{21}$$

$$Q^2_{kk'}(h,h') = \frac{k_s}{\mu}\int_{S_2} \operatorname{Re}\,\boldsymbol{\chi}_{k'}(h';\mathbf{r}_0)\cdot\mathbf{t}(\boldsymbol{\chi}^{\dagger}_{k}(h;\mathbf{r}_0))\,\mathrm{d}S\,, \tag{22}$$

$$Q_{nn'} = \frac{k_s}{\mu}\int_{S_1} \operatorname{Re}\,\boldsymbol{\psi}_{n'}(\mathbf{r})\cdot\mathbf{t}(\boldsymbol{\psi}_{n}(\mathbf{r}))\,\mathrm{d}S\,. \tag{23}$$

Regular functions in both places in equations (21)–(23) will similarly define $\operatorname{Re} Q^0_{kk'}(h,h')$, $\operatorname{Re} Q^2_{kk'}(h,h')$ and $\operatorname{Re} Q_{nn'}$. When writing equations (17)–(20) in their present form we have also made explicit use of the fact that the integrations in the z-direction in the integrals over S_0 and S_2 can be carried out analytically (since S_0 and S_2 have constant cross sections). These integrations give essentially the delta function $\delta(h-h')$ which then enables us to perform some of the h-integrations and thus we can write $Q^0_{kk'}(h)$ instead of $Q^0_{kk'}(h,h')$ and so on. The Q matrix elements for an infinite circular cylindrical surface, as defined by equations (21) and (22), have been calculated in Ref. [13] and we will not reproduce or comment any further on them here. However, for the obstacle, according to equation (23), we will return to the subject later on when we specify the shape of its surface.

The next step in the derivation will now be to solve equations (17) and (18) for $\gamma^0_{k'}(h)$ and $\gamma^2_{k'}(h)$ and then insert the results into equations (19) and (20). After introducing a number of new quantities, which are specified below, this yields

$$a_n - A_n - \sum_{n'n''} R_{nn'}T_{n'n''}c_{n''} + c_n = 0\,, \tag{24}$$

$$\begin{aligned}\mathbf{u}^s(\mathbf{r}) &= \mathbf{u}^{s,\mathrm{dir.}}(\mathbf{r}) + \mathbf{u}^{s,\mathrm{anom.}}(\mathbf{r})\\ &= \mathbf{u}^{s,\mathrm{dir.}}(\mathbf{r}) + \sum_{nn'}\mathscr{F}_n(\mathbf{r})T_{nn'}c_{n'} - \sum_{nn'}\boldsymbol{\psi}_n(\mathbf{r})T_{nn'}c_{n'}\,.\end{aligned} \tag{25}$$

Solving equation (24) for the coefficients c_n and inserting it into equation (25) then determines the scattered field which is separated into two parts. The direct scattered field, $\mathbf{u}^{s,\mathrm{dir.}}$, is the scattered field in the absence of the cavity, S_1, and the anomalous part of the scattered field, $\mathbf{u}^{s,\mathrm{anom.}}$, reflects the presence of the cavity.

Turning to the new quantities introduced in equations (24) and (25) we start by giving the form of the direct scattered field

$$\begin{aligned}\mathbf{u}^{s,\mathrm{dir.}}(\mathbf{r}) = \sum_{kk'}\int_{-\infty}^{\infty}\frac{\mathrm{d}h}{k_s}\\ \{-\boldsymbol{\chi}_k(h;\mathbf{r}_0)M^3_{kk'}(h)a^0_{k'}(h) + \boldsymbol{\chi}_k(h;\mathbf{r}_0)M^4_{kk'}(h)a^2_{k'}(h)\\ + \operatorname{Re}\chi_k(h;\mathbf{r}_0)M^1_{kk'}(h)a^0_{k'}(h) - \operatorname{Re}\boldsymbol{\chi}_k(h;\mathbf{r}_0)M^2_{kk'}(h)a^2_{k'}(h)\}\,.\end{aligned} \tag{26}$$

Here we have introduced (written in short-hand matrix notation)

$$M^1 = \mathscr{R}^2(1-\mathscr{R}^0\mathscr{R}^2)^{-1}\mathscr{R}^0\,, \tag{27}$$

$$M^2 = \mathscr{R}^2(1-\mathscr{R}^0\mathscr{R}^2)^{-1}\,, \tag{28}$$

$$M^3 = (1-\mathscr{R}^0\mathscr{R}^2)^{-1}\mathscr{R}^0\,, \tag{29}$$

$$M^4 = (1-\mathscr{R}^0\mathscr{R}^2)^{-1}\mathscr{R}^0\mathscr{R}^2\,, \tag{30}$$

where

$$\mathscr{R}^{0}_{kk'}(h) = \sum_{k''} \operatorname{Re} Q^{0}_{kk''}(h)((Q^{0})^{-1})_{k''k'}(h)\,, \tag{31}$$

$$\mathscr{R}^{2}_{kk'}(h) = \sum_{k''} Q^{2}_{kk''}(h)(\operatorname{Re} Q^{2})^{-1})_{k''k'}(h)\,, \tag{32}$$

are the reflection matrices for the inner surface, S_0, from the outside and for the outer surface, S_2, from the inside, respectively. The multiple reflections between the surfaces S_0 and S_2 are thus described by the matrices M^{ν}, $\nu = 1, 2, 3, 4$. This allows for explicit interpretation of the terms in the expression for the direct scattered field. For instance, the first term in equation (26) describes the contribution that is first reflected by the inner surface, then multiply reflected and finally again reflected by the inner surface. The transition matrix, $T_{nn'}$, for the cavity, S_1, is defined in the conventional way

$$T_{nn'} = -\sum_{n''} \operatorname{Re} Q_{nn''}(Q^{-1})_{n''n'}\,, \tag{33}$$

and the coefficients c_n by

$$c_n = i \sum_{n'} Q_{nn'}\beta_{n'}\,. \tag{34}$$

Furthermore, we have introduced what might be called the spherical projection and translation of the multiply reflected incident field

$$\begin{aligned} A_n = \sum_{kk'k''} \int_{-\infty}^{\infty} \frac{\mathrm{d}h}{k_s} C^{\dagger}_{nk''}(h) \\ \{P_{k'k''}(h;\mathbf{d})M^{3}_{k'k}(h)a^{0}_{k}(h) - P_{k'k''}(h;\mathbf{d})M^{4}_{k'k}(h)a^{2}_{k}(h) \\ - R_{k'k''}(h;\mathbf{d})M^{1}_{k'k}(h)a^{0}_{k}(h) + R_{k'k''}(h;\mathbf{d})M^{2}_{k'k}(h)a^{2}_{k}(h)\}\,, \end{aligned} \tag{35}$$

and the spherical projection and translation of the multiple reflection matrices

$$\begin{aligned} R_{nn'} = \sum_{kk'k''k'''} \int_{-\infty}^{\infty} \frac{\mathrm{d}h}{k_s} C^{\dagger}_{nk'''}(h) \\ \{-P_{k''k'''}(h;\mathbf{d})M^{3}_{k''k'}(h)P_{kk'}(h;-\mathbf{d}) + P_{k''k'''}(h;\mathbf{d})M^{4}_{k''k'}(h)R_{kk'}(h;-\mathbf{d}) \\ + R_{k''k'''}(h;\mathbf{d})M^{1}_{k''k'}(h)P_{kk'}(h;-\mathbf{d}) - R_{k''k'''}(h;\mathbf{d})M^{2}_{k''k'}(h)R_{kk'}(h;-\mathbf{d})\}C_{n'k}(h)\,. \end{aligned} \tag{36}$$

Finally, in the expression for the anomalous part of the scattered field, we have also introduced the vector field

$$\begin{aligned} \mathscr{F}_n(\mathbf{r}) = \sum_{kk'k''} \int_{-\infty}^{\infty} \frac{\mathrm{d}h}{k_s} \\ \{\boldsymbol{\chi}_k(h;\mathbf{r}_0)M^{3}_{kk''}(h)P_{k'k''}(h;-\mathbf{d}) - \boldsymbol{\chi}_k(h;\mathbf{r}_0)M^{4}_{kk''}(h)R_{k'k''}(h;-\mathbf{d}) \\ - \operatorname{Re}\boldsymbol{\chi}_k(h;\mathbf{r}_0)M^{1}_{kk''}(h)P_{k'k''}(h;-\mathbf{d}) + \operatorname{Re}\boldsymbol{\chi}_k(h;\mathbf{r}_0)M^{2}_{kk''}(h)R_{k'k''}(h;-\mathbf{d})\}C_{nk'}(h)\,. \end{aligned} \tag{37}$$

Specifying the incident field (which is the subject of the next section), determines the expansion coefficients a_n, $a^{0}_{k}(h)$ and $a^{2}_{k}(h)$. Also, employing the explicit expressions for the

basis, translation and transformation functions the various quantities introduced above may be written out in greater detail. However, this gives rise to very lengthy expressions and will not be described here.

III. The source

In this section we consider the incident field and its source which is chosen as a (time harmonic) point force, $\mathbf{F}$, acting at the point $\mathbf{r}_t$ and perpendicular to the outer cylindrical surface, S_2, of the pipe. We place the force below the inhomogeneity and consider the case when it acts at $(x_{0t}, y_{0t}, z_{0t}) = (a_2, 0, z_{0t})$, i.e. we choose a negative value of z_{0t} (cf. Fig. 1). The cylindrical coordinates, with respect to the origin O_0, are then

$$\begin{aligned} \rho_{0t} &= a_2 \\ \varphi_{0t} &= 0 \\ z_{0t} &= z_{0t} \end{aligned} \tag{38}$$

and the spherical coordinates, with respect to the origin O_1, are r_{1t}, θ_{1t}, φ_{1t} where

$$\begin{aligned} r_{1t}^2 &= (a_2 - d)^2 + z_{1t}^2 \\ \theta_{1t} &= \arccos(z_{1t}/r_{1t}) \\ \varphi_{1t} &= 0\,. \end{aligned} \tag{39}$$

The displacement field at the point $\mathbf{r}$ due to this point force is easily obtained from the free space Green tensor as

$$\mathbf{u}^i(\mathbf{r}) = \frac{k_s}{\mu}\,\mathbf{F}\cdot\mathbf{G}(\mathbf{r}, \mathbf{r}_t)\,. \tag{40}$$

Expanding $\mathbf{G}(\mathbf{r}, \mathbf{r}_t)$ in spherical or cylindrical vector waves according to equations (9) and (10), and then comparing with the field expansions according to equations (11)–(13), enable us to identify the expansion coefficients

$$a_n = i\,\frac{k_s}{\mu}\,\mathbf{F}\cdot\boldsymbol{\psi}_n(\mathbf{r}_{1t}) \tag{41}$$

$$a_k^0(h) = i\,\frac{k_s}{\mu}\,\mathbf{F}\cdot\boldsymbol{\chi}_k^{\dagger}(h; \mathbf{r}_{0t}) \tag{42}$$

$$a_k^2(h) = i\,\frac{k_s}{\mu}\,\mathbf{F}\cdot\operatorname{Re}\boldsymbol{\chi}_k^{\dagger}(h; \mathbf{r}_{0t})\,. \tag{43}$$

These expressions are the same as in [13] (with the proper Hankel or Bessel function in equations (42) and (43)). A characteristic of the vector basis functions, notable at this point, is that they decouple into basis functions which are symmetric ('even') or antisymmetric ('odd') in φ. With our choice of force, only the symmetric group is excited and this, in turn, leads to a reduction of the indices contained in the multiple indices n and k (since then specifying τ also implicitly determines σ, i.e., we have τ, $\sigma = 1$, odd; 2, even; 3, even).

IV. Numerical examples

Before discussing any numerical examples we first note that the integrands in A_n, $R_{nn'}$ and $\mathcal{F}_n$, cf. equations (35), (36) and (37), have both poles and cuts on the real h-axis. Consequently, the integration contour has to be deformed into some contour in the second and fourth quadrants and a suitable choice is (see Fig. 2)

$$ha_0 = t - i\alpha t \exp(-\beta|t|), \qquad t \in (-\infty, \infty), \quad \alpha, \beta > 0. \tag{44}$$

This contour passes through the origin and it has a maximum (minimum) for $t = -1/\beta$ ($t = 1/\beta$). Furthermore, it approaches the real h-axis in the appropriate quadrants for large $|t|$. From numerical experimentation, good convergence is obtained with $\alpha = 1/k_s a_0$ and $\beta = 1/k_s a_2$. The computations have been carried out for frequencies up to $k_s a_0 = 10$ and we have chosen to put $k_s = 2k_p$ which corresponds to Poisson's ratio $\nu = 1/3$. Recalling that the parity index, σ, is implicitly contained in the mode index, τ, and exploiting the fact that the matrices appearing in equations (35)–(37) are diagonal in some of the indices (the transformation matrix $C_{nk'}$ and the multiple reflection matrices $M^{\nu}_{kk'}$ are diagonal in the m index and the translation matrices, $P_{kk'}$ and $R_{kk'}$, are diagonal in τ) the infinite summations are reduced to summations over τ, τ' and m. These summations have been truncated at $m_{max} = 30$ at most. A 200-point Gauss–Legendre quadrature has then proved to be sufficient when computing each of the above-mentioned integrals for $t \in (-\infty, 0)$ and $t \in (0, \infty)$. Regarding the truncations for the anomalous part of the scattered field as given by equation (25), it is sufficient to take $m_{\max} = l_{\max} = 4$ for $k_s a_0 < 5$ and $m_{\max} = l_{\max} = 5$ for $5 < k_s a_0 < 10$.

The integration contour given in equation (44) has, for the same reason as above, also been used to compute the direct part of the scattered field, $\mathbf{u}^{s,\mathrm{dir}}$, defined in equation (26). The ρ- and z-components of this field are difficult to handle numerically due to slowly convergent parts of the integrands. However, these parts can be extracted and integrated analytically by means of the integral (which is easily computed by means of ordinary calculus of residues)

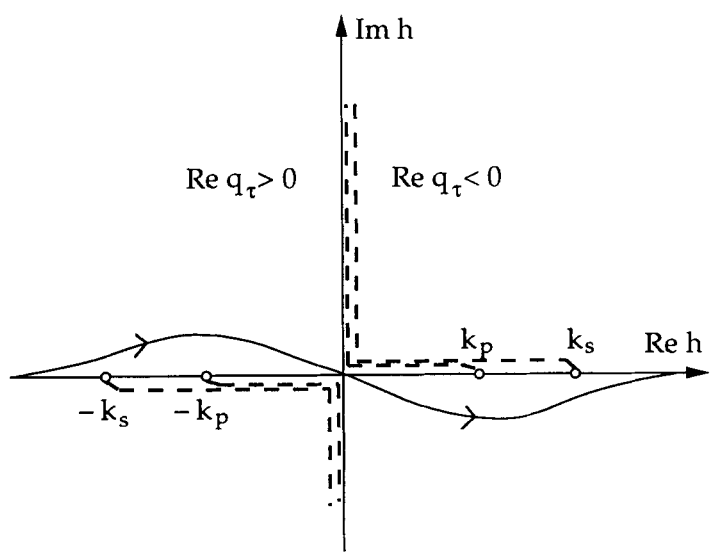

Fig. 2. Cuts (---) and integration contour in the complex h-plane.

$$\int_{-\infty}^{\infty} \frac{x \sin \alpha x}{x^2 + \beta^2} \, dx = \pi \, e^{-\alpha\beta}, \qquad \alpha > 0, \quad \mathrm{Re}\, \beta > 0. \tag{45}$$

The remaining integrals are computed with a 1000-point Gauss–Legendre quadrature. Using the same truncation ($m_{\max} = 30$ at most) as above, the components of the direct scattered field are then computed.

We have done computations when the inhomogeneity is a spherical cavity or an open circular crack (oriented in the xy-plane, i.e. the crack normal is parallel to the symmetry axis of the pipe) and, as mentioned earlier, this requires the knowledge of its T matrix. For the spherical cavity the T matrix has been well known for many years (it was first given by Waterman [1]) and for the circular crack it was recently presented by Boström and Eriksson [15]. Therefore, we shall not explore this subject any further here except for one remark about the boundary conditions which we have applied. The vanishing of the surface traction for the obstacle is by no means an essential restriction as far as the formal derivation of Section II is concerned. Other boundary conditions will just enter into the T matrix via the definition of the Q matrix elements according to equation (23). It may also be remarked that the T matrix can be obtained by other methods than the null field approach. The circular crack of Ref. [15], where a direct integral equation method is employed (and no Q matrix is involved), provides an example of this.

In the numerical examples we have chosen a pipe whose wall thickness is four tenths of its inner radius and with the obstacle (sphere or crack with radius denoted by b) centered in the pipe wall. All lengths are measured relative to the inner radius a_0 and thus the outer radius is $a_2 = 1.4a_0$ and the distance between the origins is $d = 1.2a_0$ (cf. Fig. 1). Furthermore, the point force is applied at a distance $0.2a_0$ just below the obstacle so that $(x_{0t}, y_{0t}, z_{0t}) = (1.4a_0, 0, -0.2a_0)$ and the field is evaluated on the pipe surface at the same distance and the same side above the obstacle, i.e. at $(x_0, y_0, z_0) = (1.4a_0, 0, 0.2a_0)$.

The process of solving equation (24) for the coefficients c_n involves the inversion of the matrix (written in a formal notation) $1 - RT$. In the numerical procedure this matrix inversion is accomplished by employing a Neumann series expansion.

The numerical computations have been tested as far as possible. Thus, the reflection matrices, $\mathscr{R}^0$ and $\mathscr{R}^2$, are tested for symmetry and 'hermiticity' which, in turn, are consequences of reciprocity and energy conservation (this is further commented on in Ref. [13]). Furthermore, the symmetry of the spherical projection and translation of the multiple reflection matrices, i.e. $R_{nn'}$, and the reciprocity of the anomalous part of the scattered field are also checked. The latter property means that the ρ-component of the anomalous field remains unchanged if we interchange the location of the source and the point of evaluation.

First we consider the normal component of the direct scattered field, i.e. as if no inhomogeneity is present, as a function of frequency $k_s a_0$. The computations are performed in steps of 0.01 in the frequency range $0.1 \leq k_s a_0 \leq 10.0$ and the result is shown in Fig. 3. The very pronounced peaks, which is the most striking feature in the figure, correspond to the cut-offs of the waveguide modes of the pipe for different values of the m index. Then by placing the inhomogeneity in the pipe and turning to the anomalous part of the scattered field, the corresponding frequency domain computations have been carried out. Due to the large computer time consumed, the frequency steps are now made coarser and the computations are thus performed in steps of 0.05 starting from $k_s a_0 = 0.05$. Figure 4 shows the result of such a computation for a spherical cavity of radius $b = 0.1a_0$ and Figs. 5–7 for an open circular crack of radius $b = 0.1a_0$, $b = 0.15a_0$ and $b = 0.2a_0$, respectively. The cut-off

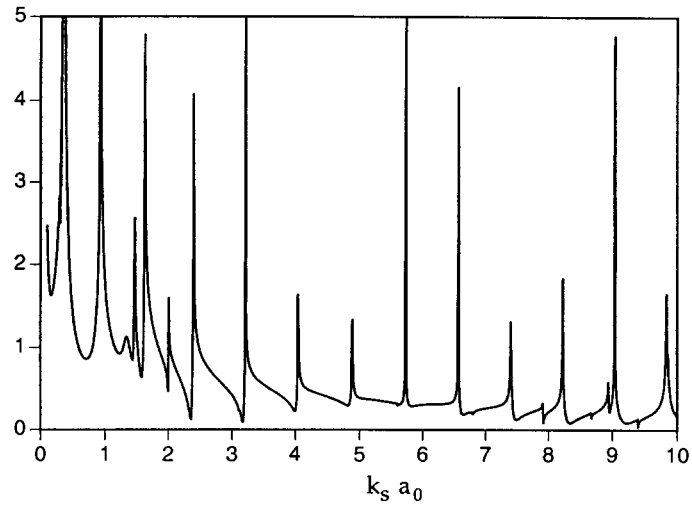

Fig. 3. Absolute value of the normal component for the direct scattered displacement field, as a function of frequency $k_s a_0$, on the outer surface of a circular cylindrical pipe.

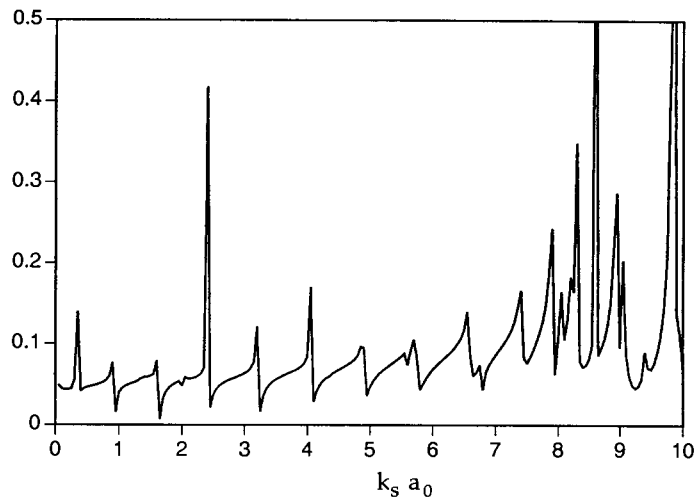

Fig. 4. Absolute value of the normal component for the anomalous scattered displacement field, as a function of frequency $k_s a_0$, on the outer surface of a circular cylindrical pipe with an embedded spherical cavity of radius $b/a_0 = 0.1$.

peaks from Fig. 3 also appear at the same frequencies in these figures although not always as well pronounced in this coarser frequency spacing. A general conclusion that can be drawn from these figures is that the sphere seems to have a greater influence on the anomalous field than does the crack (at least when the crack is oriented in the way considered here). Also, the cut-off peaks are broader, and thus become more pronounced, in the sphere case. The situation shown in Fig. 7 also requires a special remark since it deals with the extreme configuration where the diameter of the crack precisely equals the thickness of the pipe wall. Thus, there is one point on the inner and one on the outer surface where the crack just touches the respective surfaces. Examining Figs. 4–6 we note that the region around and above $k_s a_0 = 8.0$ displays a very sensitive behavior. For the extreme case of a surface

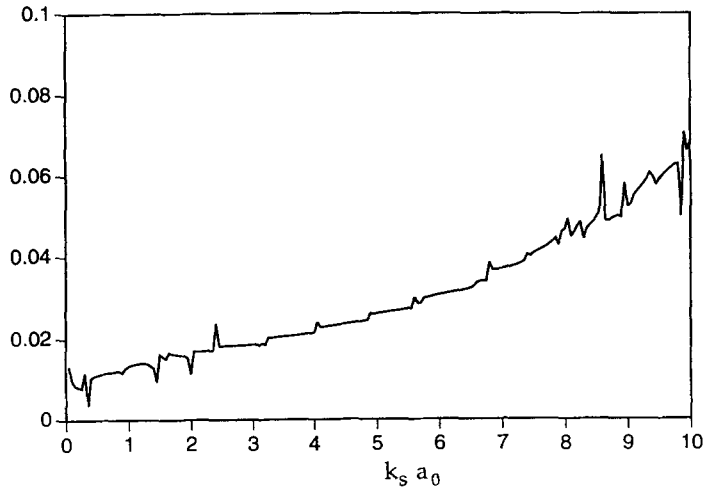

Fig. 5. Absolute value of the normal component for the anomalous scattered displacement field, as a function of frequency $k_s a_0$, on the outer surface of a circular cylindrical pipe with an embedded open circular crack of radius $b/a_0 = 0.1$.

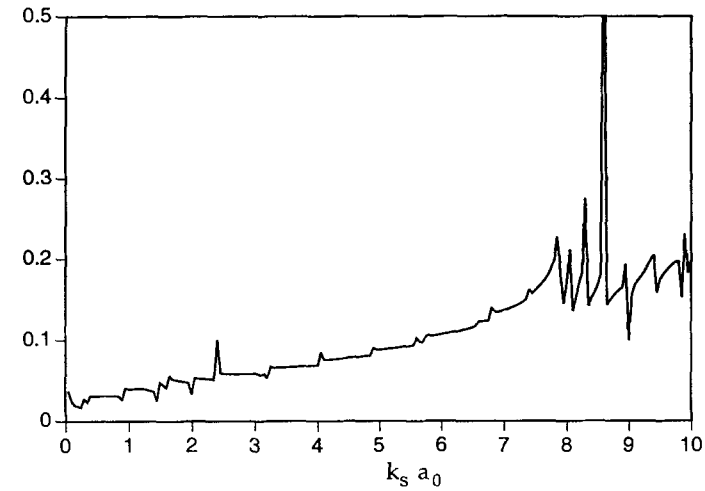

Fig. 6. The same as Fig. 5 but with a crack of radius $b/a_0 = 0.15$.

touching crack we have not, by increasing truncations, been able to achieve stable values in this region and the computations have thus been cut off at $k_s a_0 = 7.5$ as shown in Fig. 7.

Having computed the displacement field in the frequency domain we can obtain the time domain solution by a Fourier integration in frequency. We therefore assume that the source has delta function dependence on time, and to restrict the frequency range we place a filter at the receiver. This filter is chosen as

$$f(\omega) = \sin^2\left(\frac{\omega - \omega_1}{\omega_2 - \omega_1}\pi\right), \tag{46}$$

where ω_1 and ω_2 are the lower and upper boundary of the frequency band. Apart from its simple form it also has the advantage of really using most of the frequency band. Exploiting the fact that the fields should be real we thus have

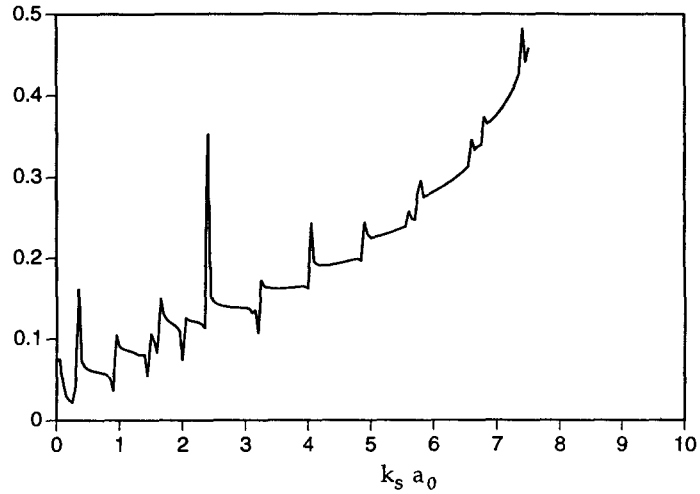

Fig. 7. The same as Fig. 5 but with a crack of radius $b/a_0 = 0.2$.

$$\mathbf{u}(\mathbf{r}, t) = \int_{\omega_1}^{\omega_2} f(\omega)\, \mathrm{Re}\{\mathbf{u}(\mathbf{r}, \omega)\, \mathrm{e}^{-i\omega t}\}\, \mathrm{d}\omega\,, \tag{47}$$

where **u** could be any of the displacement fields of interest.

The numerical integration in equation (47) is carried out by the simplest possible integration scheme, i.e. the trapezoidal rule. For comparison, all the computations have been peformed for the same frequency band $0.05 \leq k_s a_0 \leq 7.5$ (with $k_s a_0$ in steps of 0.05) and with the dimensionless time $c_s t/a_0$ in steps of 0.05 ($c_s = \omega/k_s$ is the transverse or shear wave speed). For the three different cracks of Figs. 5–7 the corresponding time domain solutions have been computed. The result for a crack of radius $b/a_0 = 0.1$ is presented in Fig. 8 which thus shows the normal component of the anomalous field, at our point of evaluation, as a

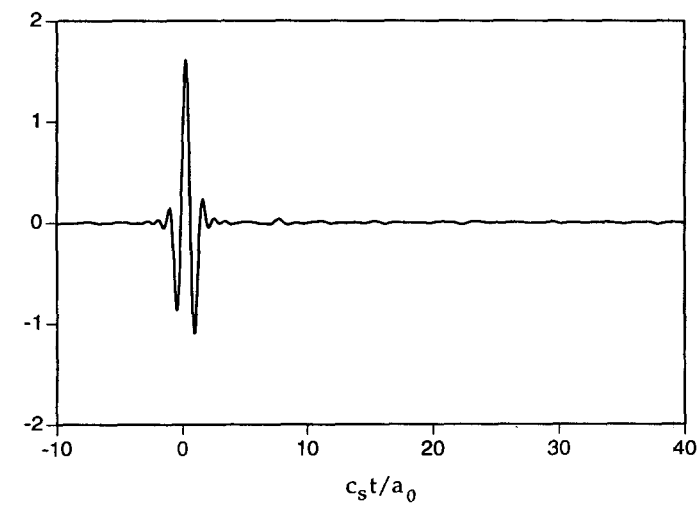

Fig. 8. The normal component of the anomalous scattered displacement field, as a function of time $c_s t/a_0$, on the outer surface of a circular cylindrical pipe with an embedded open circular crack of radius $b/a_0 = 0.1$.

function of time (the general behavior for the other two cracks are the same as in Fig. 8). As seen in the figure, there is a small flutter even a considerable time after the main pulse and this is due to both insufficient numerical accuracy and the presence of the sharp frequency cut-offs. This behavior due to the cut-offs becomes even more apparent when we try to plot the time domain solution for the anomalous field in the sphere case or for the direct field.

V. Concluding remarks

In the present paper the null field approach has been extended to the problem of a bounded inhomogeneity in a thick-walled pipe excited by a point force applied to its outer surface. A characteristic feature of this problem is that it is non-rotationally symmetric, both in the purely geometrical sense, on account of the inhomogeneity, and as a result of the applied point force. Another feature which makes the present problem more complicated as compared to the cylindrical rod treated in Ref. [13] is, of course, the presence of an additional scattering surface. This complexity is apparent when accounting for the explicit forms of the participating quantities in a comparison of the formally similar solutions of the present work and Ref. [13]. As a result the computer effort needed here is also considerable.

As mentioned earlier, the derivation presented here is valid for different inhomogeneities, both with regard to shape and boundary conditions. Once provided with the proper transition matrix, it can be fitted into our numerical scheme and, by now, the items in the library of such matrices are numerous.

Acknowledgements

The author wishes to thank Prof. A. Boström for encouragement and valuable discussions during the progress of the present work. The permission to use the computer program for the penny-shaped crack, developed by Prof. Boström and Dr. A. Eriksson, is also gratefully appreciated.

Thanks are also due to Dr. P. Olsson for suggesting several improvements in the language.

References

1. P.C. Waterman, Matrix theory of elastic wave scattering. *J. Acoust. Soc. Am.* 60 (1976) 567–580.
2. P.C. Waterman, Matrix theory of elastic wave scattering. II. A new conservation law. *J. Acoust. Soc. Am.* 63 (1978) 1320–1325.
3. Y.-H. Pao and V. Varatharajulu, Scattering matrix for elastic waves. I. Theory. *J. Acoust. Soc. Am.* 60 (1976) 556–566.
4. V.V. Varadan, Scattering matrix for elastic waves. II. Application to elliptic cylinders. *J. Acoust. Soc. Am.* 63 (1978) 1014–1024.
5. S. Ström, Introduction to integral representations and integral equations for time-harmonic acoustic, electromagnetic and elastodynamic wave fields. In V.V. Varadan, A. Lakhtakia and V.K. Varadan (eds), *Acoustic, Electromagnetic and Elastic Wave Scattering*. North-Holland, Amsterdam (1991) Vol. 1.
6. A. Boström and G. Kristensson, Elastic wave scattering by a three-dimensional inhomogeneity in an elastic half space. *Wave Motion* 2 (1980) 335–353.
7. A. Boström and A. Karlsson, Broad-band synthetic seismograms for a spherical inhomogeneity in a many-layered half space. *Geophys. J. R. Astr. Soc.* 89 (1987) 527–547.

8. A. Karlsson, Scattering of Rayleigh Lamb waves from a 2d-cavity in an elastic plate. *Wave Motion* 6 (1984) 205–222.
9. A. Boström and A. Karlsson, Point-force excitation of an elastic plate with an embedded cavity. *J. Appl. Mech.* 52 (1985) 937–942.
10. A. Boström, Transmission and reflection of acoustic waves by an obstacle in a waveguide. *Wave Motion* 2 (1980) 167–184.
11. S. Olsson, Scattering of acoustic waves by a sphere outside an infinite circular cylinder. *J. Acoust. Soc. Am.* 88 (1990) 515–524.
12. S. Olsson, Transmission and reflection of elastic waves by a spherical obstacle in an infinite circular cylindrical rod. *Comm. Div. Mech.* Division of Mechanics, CTH, Göteborg (1992).
13. S. Olsson, Point force excitation of an infinite circular cylinder with an embedded spherical cavity. *J. Acoust. Soc. Am.* 93 (1993) 2479–2488.
14. A. Boström, G. Kristensson and S. Ström, Transformation properties of plane, spherical and cylindrical scalar and vector wave functions. In: V.V. Varadan, A. Lakhtakia and V.K. Varadan (eds), *Acoustic, Electromagnetic and Elastic Wave Scattering*. North-Holland, Amsterdam (1991) Vol. 1.
15. A. Boström and A. Eriksson, Scattering by two penny-shaped cracks with spring boundary conditions. *Comm. Div. Mech.* 1992:4, Division of Mechanics, CTH, Göteborg (1992; accepted for publication in *Proc. R. Soc. Lond. A*).